Mechanistic Study of Apatite Formation on Bioactive Glass Surface Using ^{31}P Solid-State NMR Spectroscopy

Kyle S. K. Lin,[†] Yao-Hung Tseng,[†] Yun Mou,[†] Yu-Chuan Hsu,[‡] Chia-Min Yang,[‡] and Jerry C. C. Chan*[,†]

Department of Chemistry, National Taiwan University, No. 1, Section 4, Roosevelt Road, Taipei, Taiwan, and Department of Chemistry, National Tsing Hua University, 101, Section 2 Kuang Fu Road, Hsinchu, Taiwan

Received March 25, 2005. Revised Manuscript Received June 11, 2005

The molecular mechanism of apatite formation on bioactive glass surface is studied using the techniques of XRD, EDX, SEM, FT-IR, and solid-state ^{31}P NMR. Using the sol−gel method a bioactive glass system containing glass beads of 2 to 3 microns in size is prepared with the composition containing 30% CaO − 70% SiO_2. Our experimental data support the apatite formation mechanism proposed by Hench concerning the precipitation and crystallization of calcium phosphate. The phosphate ions initially deposited on the glass surface are largely in amorphous phase and have substantial amount of water molecules in the surrounding. As the soaking time in simulated body fluid increases, some of the water molecules diffuse out of the phosphate lattice, leading to the formation of a crystalline phase. Our data show that the structure of the crystalline phase is different from type B carbonate apatite but similar to hydroxyapatite.

Introduction

Glasses that are bioactive must exhibit a certain solubility to allow the necessary reactions to take place between the living tissues and the glass surface. Nowadays, it is generally accepted that the bonding of silica-glass to living tissue is primarily due to the formation of a mineral layer similar in composition to hydroxyapatite (HAp, $Ca_{10}(PO_4)_6(OH)_2$) on the glass surface.[1,2] A general mechanism of apatite formation on bioactive surfaces had been proposed by Hench and co-workers.[1,2] Accordingly, the process is divided into five stages: (i) Surface dealkalization by cation exchange with H^+, leading to a high pH local environment; (ii) Loss of soluble silica in the form of $Si(OH)_4$; (iii) Repolymerization of $Si(OH)_4$ to form a SiO_2-rich layer; (iv) Precipitation of Ca^{2+} and PO_4^{3-} ions in the silica-rich layer to form an amorphous $CaO-P_2O_5$ film; (v) Crystallization of the amorphous film by incorporation of OH^- or CO_3^{2-} anions. Numerous in-vitro studies had been carried out to understand the apatite formation process on the bioactive glasses soaked in simulated body fluid (SBF). In particular, the studies of binary $CaO-SiO_2$ glasses by Vallet-Regí and co-workers have shown that the Ca/P ratio varies from 1.6 in the apatite core to 1.2 on the apatite surface where a high population of HPO_4^{2-} ions is found.[3−5] It has also been suggested based on infrared spectroscopic data that the apatite formed on bioactive glass surface is hydroxycarbonate apatite.[3,6−8] Very recently, X-ray spectroscopy was used to demonstrate the formation of amorphous calcium phosphate at the early stage of SBF soaking.[9]

To shed more light on the stages (iv) and (v) of apatite formation, one can investigate the phosphorus environment during the course of apatite formation. In the past 15 years, solid-state NMR spectroscopy has been established as an element-selective, inherently quantitative method suited to the study of glass systems.[10] Recently, high-resolution solid-state ^{31}P NMR studies of the apatite formation on $CaO-SiO_2$ and Na_2O-SiO_2 glass systems had been reported.[11,12] The authors prepared the glass samples using the conventional melt-quench method and use the magic-angle spinning (MAS) technique to observe the ^{31}P NMR signals of the glasses with different soaking periods in SBF. However, the obtained ^{31}P NMR data do not have any significant implication because only a single ^{31}P peak was observed for each sample, where the chemical shift and line width data had very limited variation. Since many advanced solid-state NMR methods have been developed for the determination of internuclear distance,[13−15] it is possible to extract useful

[†] Department of Chemistry, National Taiwan University, No. 1, Section 4, Roosevelt Road, Taipei, Taiwan.

[‡] Department of Chemistry, National Tsing Hua University, 101, Section 2 Kuang Fu Road, Hsinchu, Taiwan.

(1) Hench, L. L.; West, J. K. *Life Chem. Reports* **1996**, *13*, 187.
(2) Hench, L. L. *J. Am. Ceram. Soc.* **1991**, *74*, 1487.
(3) Izquierdo-Barba, I.; Salinas, A. J.; Vallet-Regi, M. *J. Biomed. Mater. Res.* **1999**, *47*, 243.
(4) Martinez, A.; Izquierdo-Barba, I.; Vallet-Regi, M. *Chem. Mater.* **2000**, *12*, 3080.
(5) Vallet-Regi, M.; Perez-Pariente, J.; Izquierdo-Barba, I.; Salinas, A. J. *Chem. Mater.* **2000**, *12*, 3770.
(6) Vallet-Regi, M.; Arcos, D.; Perez-Pariente, J. *J. Biomed. Mater. Res.* **2000**, *51*, 23.
(7) Sepulveda, P.; Jones, J. R.; Hench, L. L. *J. Biomed. Mater. Res.* **2002**, *61*, 301.
(8) Yan, H. W.; Zhang, K.; Blanford, C. F.; Francis, L. F.; Stein, A. *Chem. Mater.* **2001**, *13*, 1374.
(9) Skipper, L. J.; Sowrey, F. E.; Pickup, D. M.; Fitzgerald, V.; Rashid, R.; Drake, K. O.; Lin, Z.; Saravanapavan, P.; Hench, L. L.; Smith, M. E.; Newport, R. J. *J. Biomed. Mater. Res.* **2004**, *70A*, 354.
(10) Eckert, H. *Prog. Nucl. Magn. Reson. Spectrosc.* **1992**, *24*, 159.
(11) Hayakawa, S.; Tsuru, S.; Iida, H.; Ohtsuki, C.; Osaka, A. *Phys. Chem. Glasses* **1996**, *37*, 188.
(12) Hayakawa, S.; Tsuru, K.; Ohtsuki, C.; Osaka, A. *J. Am. Ceram. Soc.* **1999**, *82*, 2155.
(13) Baldus, M. *Prog. Nucl. Magn. Reson. Spectrosc.* **2002**, *41*, 1.

10.1021/cm050654c CCC: $30.25
Published on Web 07/23/2005

structural information concerning the apatite formation using more sophisticated NMR techniques than MAS. In view of the fact that a variety of advanced NMR techniques such as $^{31}P\{^{1}H\}$ cross-polarization (CP) at variable contact delays,[16] dipolar dephasing technique,[17] heteronuclear correlation spectroscopy (HETCOR),[18−20] differential cross polarization,[21,22] and multinuclear double-resonance techniques[23] had been used to characterize the structures of synthetic hydroxyapatite, calcified tissues and apatite formation in glass matrix with tremendous success, it is somewhat surprising that ^{31}P solid-state NMR spectroscopy has not been actively employed in the study of apatite formation on bioactive glasses. Furthermore, it has been found that the rate of apatite formation on bioactive glasses depends on the texture and the dimension of the glass particles.[24,25] Therefore, one of the difficulties to study apatite formation on a sol−gel glass surface is that the sizes and morphologies of the glass debris at the micrometer scale may be very irregular. Given such irregularity in particle size, the phosphate units in different parts of the glass sample may be at different stages of apatite formation, rendering the interpretation of experimental data very difficult.

In this work, we chose to use a series of solid-state ^{31}P NMR techniques including $^{31}P\{^{1}H\}$ Lee-Goldburg spectroscopy[26,27] and ^{31}P homonuclear double-quantum (DQ) NMR[28] to monitor the formation of apatite on a CaO (30%)-SiO_2 (70%) sol−gel glass system soaked in SBF. To enhance the ^{31}P signal arising from the glass surface, poly(acrylic acid) of high molecular weight was used as a polymer template to obtain microspherical gel-silica glasses.[29] These small glass beads with uniform size and morphology are used as a high-surface area medium for NMR investigations of bioactivity. The glass preparation and the SBF soaking procedure were based on the work of Hench and co-workers.[25]

Experimental Section

Crystalline HAp was obtained from Sigma−Aldrich. All other chemicals including the monetite ($CaHPO_4$) crystalline standard were obtained from Acros Organics and used as received. The hydroxyl content of the HAp sample had been verified to be stoichiometric based on NMR spin-counting technique using the monetite sample as the reference.[20]

Table 1. Temperature Schedule for the Glass Preparation

Stage		Ramp (°C/min)	Destination temp (°C)	Duration (hr)
Aging	1	0.1	60	5.8
	2	0	60	50
	3	−0.083	35	5
Drying	1	0.1	60	5.8
	2	0.075	150	20
	3	0.025	180	20
	4	0	180	12
	5	−2.4	35	1
stabilization	1	0.875	105	1.5
	2	0.25	160	3.7
	3	0.5	500	11.3
	4	0.046	700	72.5
	5	0	700	1
	6	−1.8	40	6

Gel-Silica Glasses. The gel-silica glasses containing 30 mol % CaO and 70 mol % SiO_2 were prepared by mixing the following reagents in a 50 mL FALCON tube: 7 mL of $Si(OC_2H_5)_4$ (98%), 3.157 g of $Ca(NO_3)_2{\cdot}4H_2O$, 7.19 g of poly(acrylic acid) (MW 240000, 25 wt % in H_2O, partial sodium salt), 4.372 mL of deionized water and 0.136 mL of 14 *N* nitric acid. The tube was hermetically sealed and placed in an oven for aging. The aged sample was then dried under humid condition, where the gels were transferred from the tube to a beaker and then placed in a 6 L humidifier filled with 1.5 L of deionized water. The dried gels were then stabilized at high temperature to form glasses. The temperature schedules for aging, drying and stabilization are summarized in Table 1.

***In Vitro* Bioactivity.** Segments of 200 mg of the gel glasses were immersed in 500 mL of SBF, which was prepared by dissolving reagent-grade NaCl (136.9 mM), $NaHCO_3$ (4.18 mM), KCl (3.00 mM), $K_2HPO_4{\cdot}3H_2O$ (1.00 mM), $MgCl_2{\cdot}6H_2O$ (1.50 mM), $CaCl_2$ (3.76 mM), and Na_2SO_4 (0.50 mM) in deionized water.[30] The SBF solution was buffered at pH 7.4 using tris(hydroxymethyl)aminomethane (53.82 mM) and HCl (43.97 mM). The freshly prepared SBF solution was filtered through a 1 μm filter before use. The glass samples in SBF were incubated in an orbital shaker under 175 rpm at 37 °C for various periods: 20 min, 1 h, 3 h, 6 h, 12 h and 21.5 h. To terminate the reactions after the different soaking periods, the glass powder was collected by filtration through a 1 μm filter and then rinsed by deionized water, ethanol and acetone. The samples were dried at room temperature under reduced pressure for one to 2 days and then taken for NMR measurements.

Characterization. X-ray diffraction analysis was performed on a Mac Science 18MPX diffractometer, using Cu−Kα radiation (λ = 1.5418 Å). The field emission scanning electron microscopy (FE-SEM) and the energy-dispersive X-ray (EDX) analysis were done on a JEOL-JSM-6700F field emission scanning electron microscope (operating at 10 kV) equipped with an Oxford INCA energy-

(14) Luca, S.; Heise, H.; Baldus, M. *Accounts Chem. Res.* **2003**, *36*, 858.
(15) Schnell, I. *Prog. Nucl. Magn. Reson. Spectrosc.* **2004**, *45*, 145.
(16) Rothwell, W. P.; Waugh, J. S.; Yesinowski, J. P. *J. Am. Chem. Soc.* **1980**, *102*, 2637.
(17) Aue, W. P.; Roufosse, A. H.; Glimcher, M. J.; Griffin, R. G. *Biochemistry* **1984**, *23*, 6110.
(18) Santos, R. A.; Wind, R. A.; Bronnimann, C. E. *J. Magn. Reson. Ser. B* **1994**, *105*, 183.
(19) Kaflak-Hachulska, A.; Samoson, A.; Kolodziejski, W. *Calcif. Tissue Int.* **2003**, *73*, 476.
(20) Cho, G. Y.; Wu, Y. T.; Ackerman, J. L. *Science* **2003**, *300*, 1123.
(21) Wu, Y.; Ackerman, J. L.; Strawich, E. S.; Rey, C.; Kim, H. M.; Glimcher, M. J. *Calcif. Tissue Int.* **2003**, *72*, 610.
(22) Isobe, T.; Nakamura, S.; Nemoto, R.; Senna, M.; Sfihi, H. *J. Phys. Chem. B* **2002**, *106*, 5169.
(23) Chan, J. C. C.; Ohnsorge, R.; Meise-Gresch, K.; Eckert, H.; Holand, W.; Rheinberger, V. *Chem. Mater.* **2001**, *13*, 4198.
(24) Pereira, M. M.; Clark, A. E.; Hench, L. L. *J. Am. Ceram. Soc.* **1995**, *78*, 2463.
(25) Saravanapavan, P.; Jones, J. R.; Pryce, R. S.; Hench, L. L. *J. Biomed. Mater. Res.* **2003**, *66A*, 110.
(26) van Rossum, B. J.; de Groot, C. P.; Ladizhansky, V.; Vega, S.; de Groot, H. J. M. *J. Am. Chem. Soc.* **2000**, *122*, 3465.
(27) Ladizhansky, V.; Vega, S. *J. Chem. Phys.* **2000**, *112*, 7158.
(28) Ernst, R. R.; Bodenhausen, G.; Wokaun, A. *Principles of Nuclear Magnetic Resonance in One and Two Dimensions*. Clarendon Press: Oxford, 1987.
(29) Gallardo, J.; Galliano, P. G.; Lopez, J. M. P. *Biomaterials* **2002**, *23*, 4277.
(30) Kokubo, T.; Kushitani, H.; Sakka, S.; Kitsugi, T.; Yamamuro, T. *J. Am. Ceram. Soc.* **1990**, *78*, 2463.

dispersive X-ray spectrometer. Absorbance FT-IR spectra were collected using a Magna-IR 550 spectrometer (series II), in the range of 400−4000 cm^{-1}. The BET surface areas of the glass samples were obtained from the N_2 adsorption−desorption isotherm measured using a Micrometry Tristar system, where the samples were degassed at 200 °C under reduced pressure (10^{-3} Torr) for 16−20 h before each measurement.

Solid-State NMR. All NMR experiments were carried out at ^{31}P and ^{1}H frequencies of 121.5 and 300.1 MHz, respectively, on a Bruker DSX300 NMR spectrometer equipped with a commercial 4-mm probe. All spectra were measured at room temperature. The sample was confined to the middle 1/3 of the rotor volume using Teflon spacers. MAS frequency variation was limited to ± 3 Hz using a commercial pneumatic control unit. Chemical shifts were externally referenced to 85% phosphoric acid and TMS for ^{31}P and ^{1}H, respectively. The ^{31}P spin-relaxation times (T_1) were determined by the saturation-recovery technique. The ^{31}P MAS spectra were measured at a spinrate of 10 kHz and with 60 kHz proton decoupling. An exponential window function of 80 Hz line broadening was applied to each FID before the Fourier transformation. Recycle delay was set to 43 s. The ^{31}P spin counting experiments were performed using $Ag_7P_3S_{11}$ as the intensity standard (recycle delay 300 s). The $^{31}P\{^{1}H\}$ CPMAS experiments with variable contact times were done at a spinrate of 10 kHz. Recycle delay was set to 4 s. During the contact time the ^{1}H nutation frequency was set equal to 50 kHz and that of ^{31}P was ramped through the Hartmann−Hahn matching sideband.[31]

The $^{31}P\{^{1}H\}$ Lee-Goldburg CP heteronuclear correlation (LG-CP HETCOR) spectra were measured at a spinrate of 10 kHz. The flip angle of the pulse after the t_1 evolution is adjusted so that the spin-temperature inversion can be realized by phase alternating the first $\pi/2$ pulse. During the contact time (2 ms) the ^{1}H nutation frequency and the resonance offset were set equal to 50 and 35.35 kHz, respectively, to fulfill the Lee-Goldburg irradiation condition. Proton decoupling during the acquisition time was set to 60 kHz. Quadrature detection in the F_1 dimension was achieved by the hypercomplex approach. Typically, for each t_1 increment 32 transients were accumulated, and a total of 256 increments were done at steps of 10 μs.

The ^{31}P DQ experiments were carried out under MAS spinning frequency of 10 kHz based on the so-called HSMAS-DQ technique.[32,33] To prepare the initial spin system identically for each transient, a saturation comb was applied prior to the recovery delay (12 s). During the DQ excitation and reconversion periods, the ^{31}P $\pi/2$ and π pulses were set to 3 and 12 μs long, respectively. The π pulse trains were phase cycled according to the XY-8 scheme.[34] The DQ reconversion period was set equal to the excitation period. Proton decoupling was set to 100 and 60 kHz during the DQ excitation/reconversion periods and the acquisition time, respectively. A more detailed description of the experiment was given elsewhere.[33] The pulse sequences used for the ^{31}P-^{31}P DQ measurements and $^{31}P\{^{1}H\}$ Lee-Goldburg CP heteronuclear correlation (LG-CP HETCOR) are shown in Figure 1.

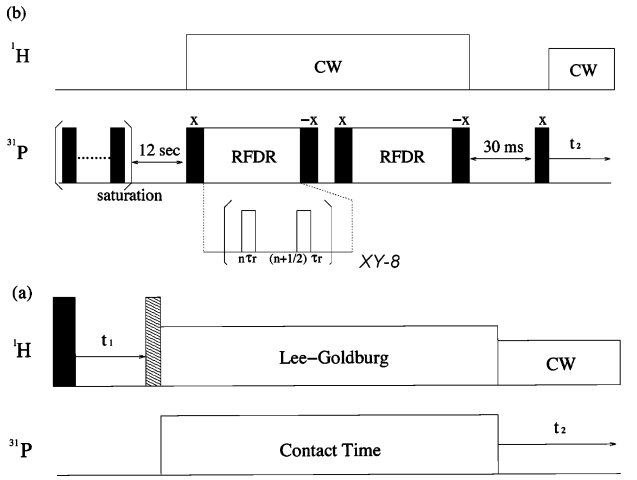

Figure 1. Pulse sequences used for the (a) $^{31}P\{^{1}H\}$ LG-CP heteronuclear correlation. The filled and open rectangles denote 90° and 180° pulses, respectively. The shaded rectangle represents a pulse with a flip angle equal to 144.7° for our spectrometer (b) ^{31}P double-quantum measurements.

Results and Analyses

Glass Preparation. The SEM image of the glass samples before SBF soaking is shown in Figure 2a, in which beads of diameter ca. 3 μm were observed. The glass beads were shown to be amorphous by XRD measurements. For comparison, another batch of glass sample was prepared using the same protocol except that no template molecules were added. The gel glasses hence obtained have very irregular sizes and morphologies (see Figure 2b), and they are not considered any further in the subsequent discussion.

SEM, EDX and BET surface areas. A series of samples were obtained by soaking the glass beads in SBF for different periods, viz. 20 min, 1 h, 3 h, 6 h, 12 h and 21.5 h. All the soaked glass samples will henceforth be labeled based on their soaking times. Referring to the SEM image of the 3-hr sample shown in Figure 3a, there are trace amounts of minerals deposited on the glass surface. As expected, the SEM images of samples with longer soaking time show that more minerals are deposited (data not shown). Figure 3b shows the SEM image of the 21.5-hr sample. The minerals deposited on the glass surface have a morphology similar to the crystal habit of apatite formed on bioactive glasses.[35,36] In principle we can use EDX to determine the Ca/P ratio of the minerals. However, the high calcium content of our base glass rendered this analysis not trivial. Since our instrument has only limited resolution, we carefully selected the mineral debris which were remote from any glass beads for our EDX analysis. The average Ca/P ratios for the 6-hr, 12-hr and 21.5-hr samples were found to be 1.47, 1.47 and 1.63, respectively. The Ca/P ratio is calculated as 1.67 based on the ideal

(31) Metz, G.; Wu, X. L.; Smith, S. O. *J. Magn. Reson. A* **1994**, *110*, 219.
(32) Oyler, N. A.; Tycko, R. *J. Phys. Chem. B* **2002**, *106*, 8382.
(33) Tseng, Y. H.; Mou, Y.; Mou, C. Y.; Chan, J. C. C. *Solid State Nucl. Magn. Reson.* **2005**, *27*, 266.
(34) Gullion, T.; Baker, D. B.; Conradi, M. S. *J. Magn. Reson.* **1990**, *89*, 479.
(35) Li, P. J.; Ohtsuki, C.; Kokubo, T.; Nakanishi, K.; Soga, N.; Nakamura, T.; Yamamuro, T. *J. Am. Ceram. Soc.* **1992**, *75*, 2094.
(36) Li, P.; Nakanishi, K.; Kokubo, T.; de Groot, K. *Biomaterials* **1993**, *14*, 963.

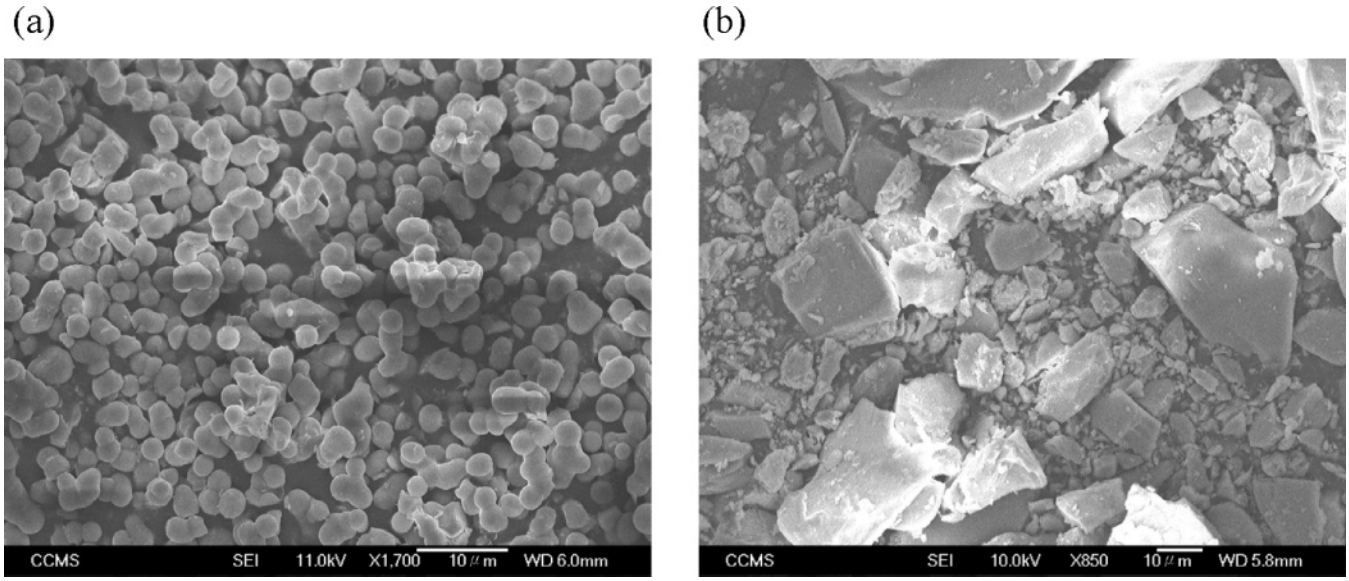

Figure 2. SEM images of the glasses prepared (a) with poly(acrylic acid)s used as the templates and (b) without template molecules.

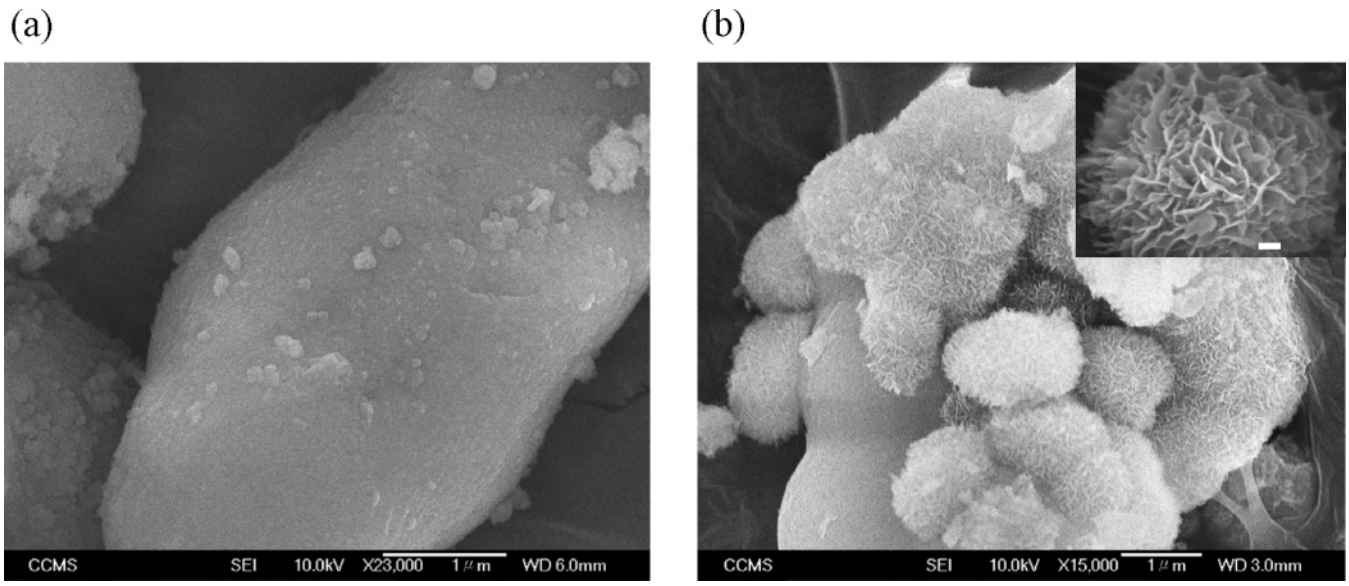

Figure 3. SEM images of the glass beads soaked in SBF for (a) 3 h and (b) 21.5 h. The scale bar of the inset is of 100 nm.

stoichiometry of pure HAp. We are not able to find any debris in the 3-hr sample even after sonification. Before soaking in SBF solution, the glass sample has a BET surface area of 140 m^2/g. As the soaking time increases, the BET surface areas of the samples eventually increase to nearly 300 m^2/g.

XRD and FT-IR. To identify the minerals formed on the glass surface, the XRD patterns of our sample series were measured. Referring to Figure 4, there are several sharp diffraction peaks (marked by dots and asterisks) clearly observed for the 1-hr, 3-hr and 6-hr samples. The peaks marked by asterisks originate from calcite but we are not able to identify the peak marked by dots (Fig. S1 of the Supporting Information). Calcite formation was also identified in a recent XRD study of binary $CaO-SiO_2$ study.[4] For the 6-hr sample, an additional broad peak at 2θ equal to 32° becomes apparent (marked by an arrow), suggesting the incipient formation of a low crystallinity apatite-like phase on the glass surface.[37] As the soaking time increases further to 21.5 h, the overall diffraction pattern becomes quite similar to that of crystalline HAp.[35,37] However, the resolution of the diffraction pattern remains poor for the 21.5-hr sample. This could be attributed to the size/imperfection/strain of the crystallites.[37,38] Together with the large BET surface area determined for our 21.5-hr sample, the apatite crystallites are likely nanosized. Figure 5 shows the FT-IR data measured for the sample series. The samples were dried at 80 °C for 18 h before the measurements. The absorption peaks corresponding to the P−O bending mode are observed in the 12-hr sample and become more intense in the 21.5-hr sample, revealing the presence of PO_4^{3-} or HPO_4^{2-} ions.[8,25,39] The peak at 875 cm^{-1} is assigned to the CO stretching of CO_3^{2-} ions.[3,7] This CO stretching peak was also clearly observed in other studies of $CaO-SiO_2$ glasses.[7,8] The OH stretch at

(37) Vallet-Regi, M.; Romero, A. M.; Ragel, C. V.; LeGeros, R. Z. *J. Biomed. Mater. Res.* **1999**, *44*, 416.
(38) Klug, H. P.; Alexander, L. E. *X-ray diffraction procedures of polycrystalline and amorphous materials*. John Wiley & Sons: New York, 1974.
(39) Takadama, H.; Kim, H. M.; Kokubo, T.; Nakamura, T. *Chem. Mater.* **2001**, *13*, 1108.

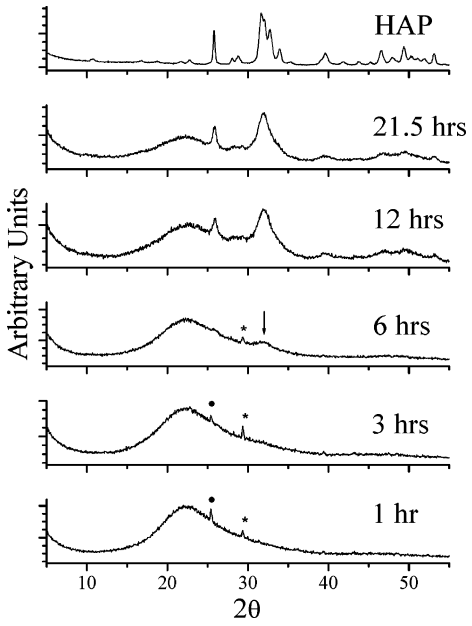

Figure 4. XRD patterns of the HAp crystalline standard and the glass samples with selected soaking periods in SBF. The peaks marked with asterisks are due to calcite. The peaks marked with filled circles are not identified. The arrow marks the onset of the diffraction peak of the apatite crystalline phase.

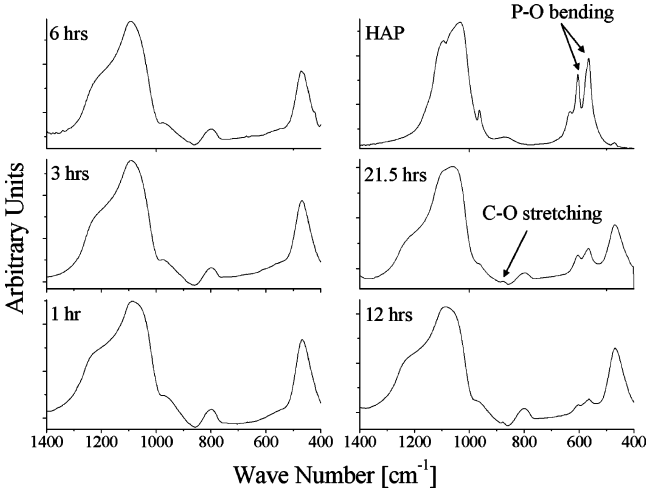

Figure 5. FT-IR spectra of the HAp crystalline standard and the glass samples with selected soaking periods in SBF.

3572 cm^{-1} is not observed for our soaked samples because of the poor crystallinity of the apatite crystallites.

^{31}P MAS NMR. The ^{31}P spin−lattice relaxation times of our sample series were ca. 35 s. All the ^{31}P MAS spectra of the sample series invariably have a major peak positioned at around 3.3 ± 0.2 ppm, which is tentatively assigned to be the PO_4^{3-} signal because the signals of HPO_4^{2-} ions in octacalcium phosphate and monetite are more shielded (≤ 1.4 ppm).[40,41] To verify that the ^{31}P signal is not arising from incomplete washing, a control sample was prepared with soaking time in SBF of 20 s only. The very weak ^{31}P signal of the control sample proves that the amounts of the PO_4^{3-} ions due to residual SBF are very minor in all the soaked samples (data not shown). The amounts of the PO_4^{3-} ions deposited on the glass surface were determined by NMR spin-counting technique. Figure 6 plots the full line widths at half-maximum ($\Delta\nu_{(1/2)}$) and the percentage by mass of PO_4^{3-} versus the soaking times. While the ^{31}P chemical shift data do not show any significant variation, there is an interesting trend in the line width data. The $\Delta\nu_{(1/2)}$ data of the 20-min, 30-min, 1-hr and 3-hr samples are ca. 5.8 ppm and decrease down to ca. 4.3 ppm for other samples with longer soaking times. The line widths were estimated by fitting the peak by a 50% Gaussian- 50% Lorentzian line shape. The error bars were estimated by comparing the fitted line widths and those measured directly at half-maximum. The line width data indicate that initially (soaking time ≤ 3 h) the phosphate ions deposited on the glass surface were largely amorphous. This interpretation is consistent with an earlier study,[42] in which the ^{31}P line width of synthetic amorphous calcium phosphate was reported to be ca. 5 ppm larger than that of crystalline HAp. As expected, the amount of PO_4^{3-} ions increases monotonically as the soaking time increases. The amount of deposited PO_4^{3-} ions reached a plateau after 12-hr soaking due to the consumption of the phosphate ions in the SBF solution.

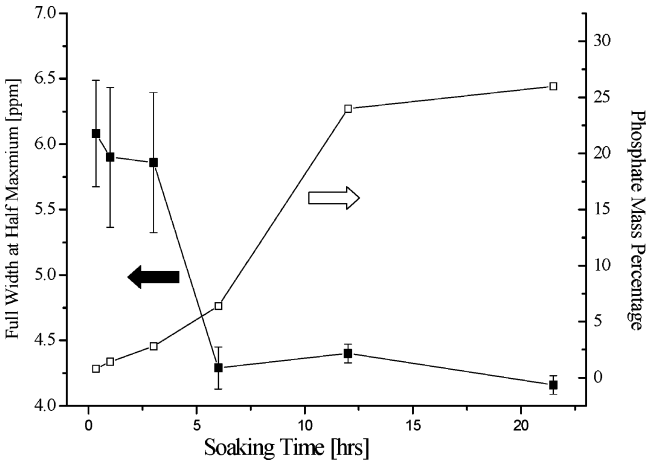

Figure 6. Plot of fullwidths at half-maximum of the ^{31}P MAS signals and the mass percentage of the phosphate ions.

^{31}P{^{1}H} LG-CP HETCOR. The proximities of the phosphate and hydrogen sites were studied by ^{31}P{^{1}H} LG-CP HETCOR. Figure 7 shows the HETCOR spectrum of the 21.5-hr sample. Since the spin diffusion among the ^{1}H spins during the CP contact time is suppressed, our data clearly show that there are at least two different phosphorus species formed on the glass surface. While the ^{31}P peak correlated with the ^{1}H signal at 0.2 ppm is readily assigned to HAp (henceforth referred to as the apatite component),[43] it is not trivial to assign the ^{31}P signal correlated with the ^{1}H signal at 5.0 ppm. Figure 8 shows the projection of Figure 7 along the ^{1}H dimension which has two salient features. First, the sideband pattern has a large span (ca. 45 kHz) but the overall sideband intensities is significantly less than the center band at 5.0 ppm. It implies that there exists another signal at 5.0 ppm which does not have any significant

(40) Tseng, Y. H.; Zhan, J. H.; Lin, K. S. K.; Mou, C. Y.; Chan, J. C. C. *Solid State Nucl. Magn. Reson.* **2004**, *26*, 99.
(41) Wu, Y. T.; Glimcher, M. J.; Rey, C.; Ackerman, J. L. *J. Mol. Biol.* **1994**, *244*, 423.
(42) Tropp, J.; Blumenthal, N. C.; Waugh, J. S. *J. Am. Chem. Soc.* **1983**, *105*, 22.
(43) Yesinowski, J. P.; Eckert, H. *J. Am. Chem. Soc.* **1987**, *109*, 6274.

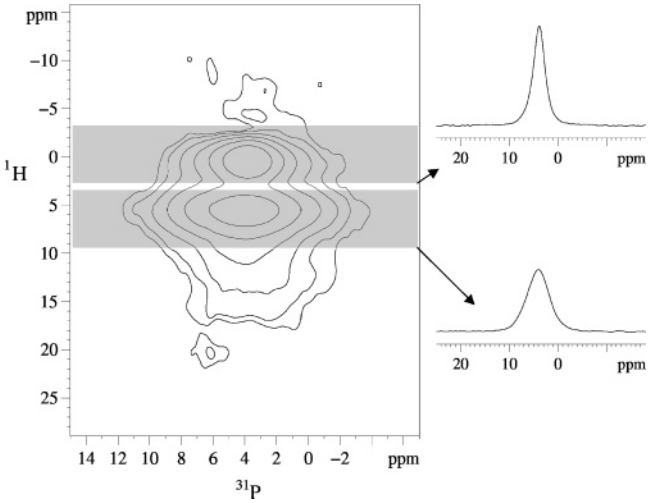

Figure 7. Two-dimensional ^{31}P{^{1}H} LG-CP HETCOR spectrum measured for the 21.5-hr sample. The projections of the shaded area along the ^{31}P dimension were shown to highlight the different $\Delta\nu_{(1/2)}$ for the two major spectral components.

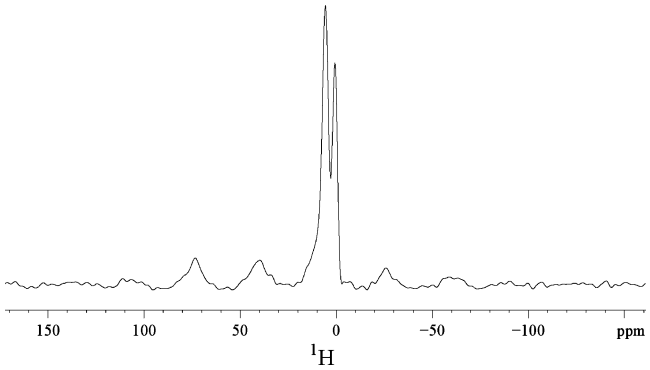

Figure 8. ^{1}H projection of the ^{31}P{^{1}H} LG-CP HETCOR spectrum of Figure 7.

spinning sideband manifold. Second, the sideband pattern is rather asymmetric compared with those arising from isolated structural water.[43] In comparison, the CP−HETCOR spectra reported for bovine cortical bone is quite similar to ours except that the H_2O signal does not have any significant spinning sidebands.[20] Therefore, we suggest that the ^{1}H signal at 5.0 ppm is due to two spectral components. The component with weaker sideband manifold is presumably due to the surface-absorbed water with weak dipolar couplings to the PO_4^{3-} ions.[20] The one with significant sideband intensities is due to the structural water hydrogen-bonded to the PO_4^{3-} ions, which may undergo the following hydrolysis reaction:

$$PO_4^{3-} + H_2O = HPO_4^{2-} + OH^-$$

The ^{31}P chemical shift value (3.2 ppm) suggests that the hydrogen bonding is modulated by molecular motions and/or chemical exchange because ^{31}P NMR measurements on octacalcium phosphate show that the isolated PO_4^{3-} ions, hydrogen bonded PO_4^{3-} ions and the HPO_4^{2-} ions have chemical shifts equal to 3.7, 2.0 and −0.2 ppm, respectively.[40] Also, it had been pointed out in a ^{31}P NMR study of nonstoichiometric HAp that HPO_4^{2-} ions undergoing molecular motions would have the same isotropic chemical shift as the PO_4^{3-} ions in HAp, and that discrete and rigid HPO_4^{2-} ions are not found in nonstoichiometric HAp samples with Ca/P ratios equal to 1.46 and 1.33.[16]

The apatite component of the LG-CP HETCOR spectrum (Figure 7) has ^{31}P $\Delta\nu_{(1/2)}$ equal to 2.8 ppm. Since the $\Delta\nu_{(1/2)}$ value of crystalline HAp was found to be 1.7 ppm, the apatite nanocrystals formed on the glass surface appears to be structurally close to crystalline HAp. The ^{31}P signal correlated to both surface and structural water signals has $\Delta\nu_{(1/2)}$ equal to 5.3 ppm (the water component), showing that the spatial arrangements of these phosphate ions are more disordered. Additional LG-CP HETCOR spectra were obtained for other glass samples with shorter soaking times. The LG-CP HETCOR spectrum of the 3-hr sample does not have any apatite component and the spectra of the 6-hr and 21.5-hr samples have very similar spectral features except that the relative intensity of the apatite component is larger for the 21.5-hr sample (Figs. S2 and S3 of the Supporting Information). Hence, the step like decrease in the line width data of the 6-hr sample (Figure 6) is due to the incipient formation of apatite crystallites. For the 21.5-hr sample, the $\Delta\nu_{(1/2)}$ value of the ^{31}P MAS signal (4.2 ppm) indicates that a significant portion of the phosphorus species still has considerable structural disorder, which is due to both the surface phosphorus and the phosphorus species in an amorphous state. Unfortunately, it is difficult to unambiguously determine the relative populations of these two components by deconvoluting the MAS spectra. In principle, one may measure a series of LG-CP HETCOR spectra with different contact times for each sample in order to monitor the changes in the CP dynamics of the different phosphate species. In view of the difficulties of controlling the water content of our samples over a long period, we do not plan to perform these extremely time-consuming experiments.

^{31}P{^{1}H} CPMAS with Variable Contact Times. To investigate the protonation state of the phosphorus species, ^{31}P{^{1}H} variable contact time CPMAS experiments were measured for our sample series and two model crystalline compounds, viz. HAp and monetite. The ^{31}P signals as a function of contact time were fitted by the following equation:

$$I(t) = I_0\{1 - \exp(-t/\tau_{CP})\}\exp(-t/T_{1\rho}^H)$$

The τ_{CP} values of HAp and monetite were found to be 795 ± 32 and 314 ± 14 μs, respectively. The $T_{1\rho}^H$ value of monetite was measured to be 9.8 ± 0.4 ms but our contact time scale (≤ 8 ms) is too short to characterize the $T_{1\rho}^H$ of HAp. As expected, in monetite the stronger ^{31}P-^{1}H and ^{1}H-^{1}H dipolar interactions result in the shorter τ_{CP} and $T_{1\rho}^H$ values, respectively. Figure 9 summarizes the τ_{CP} and $T_{1\rho}^H$ values of selected glass samples, where the raw data can be found in Fig. S4 of the Supporting Information. The τ_{CP} values of the samples with soaking times ≤ 3 h are quite similar to that measured for HAp. There is a step increase in τ_{CP} for the 6-hr sample. While the τ_{CP} values are similar for the 6-hr and the 12-hr samples, there is another increase in τ_{CP} for the 21.5-hr sample. Invariably all the τ_{CP} values are much larger than that determined for monetite. On the other hand, the $T_{1\rho}^H$ values of the soaked samples increase

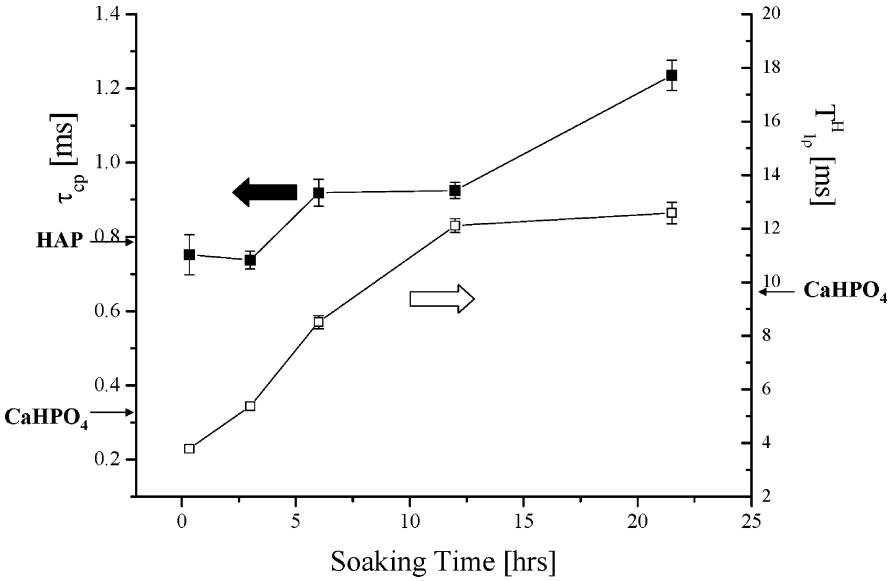

Figure 9. Plot of the τ_{CP} and $T_{1\rho}^H$ values of selected glass samples. The arrows mark the values corresponding to crystalline HAp and monetite.

gradually and reach a plateau after 12 h of SBF soaking. In an XPS study it has been concluded that a high population of HPO_4^{2-} ions is present on the surface of CaO(20%)-SiO_2-(80%) glasses after soaking in SBF.[5] Although our τ_{CP} data can completely rule out the presence of any rigid and discrete HPO_4^{2-} ions, these data remain compatible with the presence of HPO_4^{2-} ions undergoing restricted motion and/or chemical exchange. Consistent with the LG-CP HETCOR data, the relatively short $T_{1\rho}^H$ values indicate that the ^{31}P CP signals of our samples with short soaking times are mainly arising from the phosphate ions interacting with both the surface water and structural water, whereby dipolar coupling among the protons of the water molecules is significant. As the phosphate structure becomes more HAp-like, the decrease in the amount of structural water relative to the phosphate ions results in an increase in $T_{1\rho}^H$. The gradual increase in τ_{CP} reveals that the ^{31}P-^{1}H CP dynamics between the OH^- and the PO_4^{3-} species of the apatite component are weaker than that in crystalline HAp. Presumably the OH^- ions are in chemical exchange with other water molecules.

^{31}P Double-Quantum NMR. When two or more nuclear spins are close in proximity, they become coupled through the homonuclear dipole−dipole interaction. The magnitude of such interaction is inversely proportional to the third power of the internuclear distance. The so-called DQ coherence is a concerted evolution of coupled spins, which can be excited and detected under the irradiation of carefully designed rf pulse sequence. Referring to the HSMAS-DQ pulse sequence shown in Figure 1, a systematic variation in the DQ excitation and reconversion periods can be used to probe the van Vleck's second moment of the coupled spins,[44] whose magnitude depends on both the number of interacting spins and the internuclear distances:

$$M_2 = \frac{3}{5}\gamma^4\hbar^2 I(I+1)\sum_j \frac{1}{r_j^6}$$

Qualitatively, the larger the second moment, the faster the growth of the DQ signal. As a crude approximation, the build up of the DQ signals is described by a parabolic function.[45,46] By numerical simulations of multiple-spin systems, we have recently shown that the DQ signals will be attenuated by dephasing effects due to other passive spins.[33] Therefore, we chose to approximate the decay of the DQ signals by a Gaussian function for our multiple-spin systems.[47] Overall, the following empirical equation is used to fit the DQ signals as a function of excitation time:

$$I(\tau_{exe}) = A{\tau_{exe}}^2 \exp\{-{\tau_{exe}}^2/B\}$$

where the rate of the initial DQ signal buildup is described by the parameter A, which is proportional to the M_2 of the interacting nuclear spins; the constant B describes the decay of the DQ signal. The excitation profile of the DQ signals, which had been normalized with respect to the MAS signals measured under identical conditions (spinning frequency, saturation comb and relaxation delay), was fitted by the above empirical equation (Fig. S5 of the Supporting Information). The variation of the parameter A reflects the same variation in M_2. We also measured the A value for HAp so that we can calibrate the proportionality constant between A and M_2 (Table 2). Figure 10 shows the M_2 values of the soaked samples as a function of soaking time. The results indicate that initially the M_2 value of the phosphate units is about 53% of that of the crystalline HAp (M_2^{HAp}). Then, the M_2 increases to 83% of M_2^{HAp} for the 1-hr sample. As the soaking time increases further, the M_2 values increase only moderately and become eventually equal to that of crystalline HAp within experimental error. For comparison, the M_2 value determined by Ackerman and co-workers for the highly crystalline and poorly crystalline type B carbonate apatite are both equal to 75% of M_2^{HAp}.[48] Therefore, the apatite structure formed on the glass surface appears to be different

(44) Abragam, A. *Principles of Nuclear Magnetism*. Clarendon Press: Oxford, 1961.
(45) Bertmer, M.; Eckert, H. *Solid State Nucl. Magn. Reson.* **1999**, *15*, 139.
(46) Gunne, J.; Eckert, H. *Chem.-Eur. J.* **1998**, *4*, 1762.
(47) Engelsberg, M.; Norberg, R. E. *Phys. Rev. B* **1972**, *5*, 3395.

Table 2. Fitting Parameters *A* and *B* of the ^{31}P Homonuclear DQ Excitation Profiles. The Proportionality Constant between *A* and M_2 Is Calibrated by Comparing the *A* Value and the Calculated M_2 of Crystalline HAp

Sample	A (ms^{-2})	B (ms^2)	M_2 ($\times 10^6$ rad^2/s^2)
20-min	4.9 ± 0.7	5.4 ± 0.5	4.0 ± 0.6
1-hr	7.7 ± 0.7	6.5 ± 0.4	6.3 ± 0.5
3-hr	7.8 ± 0.3	7.5 ± 0.2	6.4 ± 0.3
6-hr	7.9 ± 0.7	7.8 ± 0.4	6.5 ± 0.6
12-hr	9.0 ± 0.4	7.2 ± 0.3	7.4 ± 0.4
21.5-hr	9.1 ± 0.5	6.8 ± 0.3	7.4 ± 0.4
HAp	9.4 ± 0.4	6.1 ± 0.2	7.7[a]
Octacalcium phosphate	- -	- -	6.9[a,b]

[a] Calculated values based on the X-ray structures of crystalline HAp (ref 54) and octacalcium phosphate (ref 59). [b] The average of the six phosphorus sites.

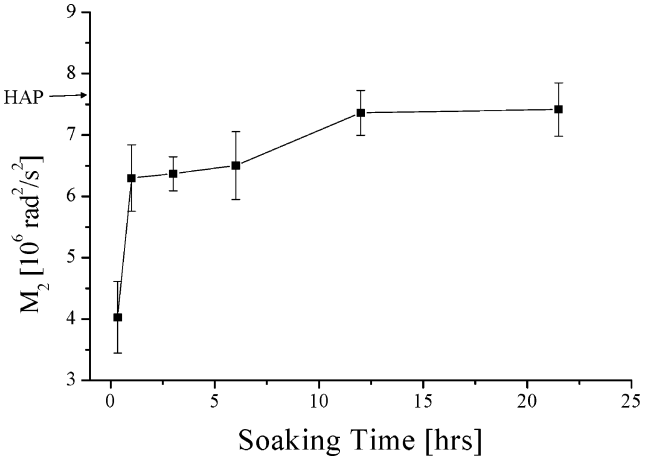

Figure 10. Plot of the ^{31}P-^{31}P second moment for selected samples. The arrow marks the value corresponding to crystalline HAp.

from that of synthetic type B carbonate apatite, in which some of the phosphate ions are substituted by carbonate ions (ca. 9% by mass).[49] We believe that the carbonate content of the apatite formed on our glass surface, if any, must be substantially less than 9% by mass. We note in passing that octacalcium phosphate has been postulated as a precursor phase of apatite formation in biomineralization. For comparison, the calculated M_2 value of octacalcium phosphate is also included in Table 2. On the other hand, since the values of the parameter *B* are affected by both the ^{31}P spin−spin relaxation times and the spatial arrangement of the interacting phosphorus species, it is difficult to interpret the data trend unequivocally.

Discussion and Conclusion

Bioactive Glass Beads. Our sol−gel glass system has the salient feature that it is rather uniform in size and morphology (Figure 2a). Furthermore, the use of high-humidity drying is expected to produce a homogeneous distribution of the calcium ions in our base glass.[50] Consequently, our experimental data should faithfully reflect the chemical environments of the phosphate ions at different stages of apatite formation, although it has been shown that the chemical composition of the apatite layer formed on bioactive glasses is very heterogeneous.[5] While glass beads of similar size (2−3 microns) have been reported earlier,[29] to our knowledge this work represents the first attempt in the literature to investigate their bioactivity.

^{31}P{^{1}H} LG-CP HETCOR Spectroscopy. ^{31}P{^{1}H} CP−HETCOR spectra have been reported for crystalline HAp and bovine cortical bone.[18−20] In particular, the ^{1}H homonuclear decoupled CP−HETCOR approach has been demonstrated for a long time.[18] This sophisticated multiple-pulse based approach, which can suppress ^{1}H-^{1}H spin diffusion during the contact time period, has not been widely applied in the study of calcified tissues because of the rather involved setup procedure. In this work, we have demonstrated that the LG-CP method, which was originally developed for the study of ^{1}H-^{13}C multiple-spin systems,[26,27] can be easily and successfully applied for the study of apatite minerals. Because the LG irradiation can effectively suppress the homonuclear dipolar coupling, our spectrum shown in Figure 7 has a much better resolution than the one measured based on the regular CP approach (data not shown). In a recent study of bone and dental materials, it has been shown that CP with very short contact time will selectively enhance the signals of the phosphorus species near the apatite surface.[48] For the sake of spectral sensitivity, however, we deliberately used a longer contact time (2 ms) for our LG-CP HETCOR measurement because LG irradiation will attenuate the polarization transfer rate considerably.[26,27] Furthermore, our glass samples after the SBF soaking were merely dried at room temperature under reduced pressure, therefore the apatites of colloidal dimensions contained a significant amount of surface-adsorbed water which might have condensed to form a "liquidlike" layer.[43] As a result, the rapid chemical exchange and molecular motions of the surface waters may also have attenuated the polarization transfer rate of the phosphorus species near the apatite surface.

^{31}P-^{31}P Second Moment. For the SBF soaking condition used in our study, heterogeneous nucleation (phosphate cluster adsorption on substrate surface) has been shown to be the predominant mechanism of HAp formation.[51] In a subsequent study, micropatterns of HAp have been obtained by modifying the electrostatic potential of the substrate surface.[52] Similarly, the growth and coalescence of crystallites adsorbed on a surface has been suggested as the mechanism for HAp formation on self-assembled monolayers.[53] Our ^{31}P-^{31}P M_2 values determined for the apatite formed on the glass surface reflects the variation in the "phosphorus density" as a function of soaking time. The M_2 values for spherical cluster sizes of 5 Å, 8 Å, 10, 15, and 20 Å were calculated to be 5.8, 7.0, 7.4, 7.6 and 7.7 $\times 10^6$ rad^2/s^2, based on the geometry of crystalline HAP.[54] These figures show that the increase in M_2 value ($\times 10^6$ rad^2/s^2) from the 20-min sample (4.0 ± 0.6) to the 1-hr sample (6.3 ± 0.5) is most likely due to a significant increase in the local

(48) Wu, Y. T.; Ackerman, J. L.; Kim, H. M.; Rey, C.; Barroug, A.; Glimcher, M. J. *J. Bone Miner. Res.* **2002**, *17*, 472.
(49) Fleet, M. E.; Liu, X. *J. Solid State Chem.* **2004**, *177*, 3174.
(50) Zhong, J.; Greenspan, D. C. *J. Biomed. Mater. Res.* **2000**, *53*, 694.
(51) Zhu, P. X.; Masuda, Y.; Yonezawa, T.; Koumoto, K. *J. Am. Ceram. Soc.* **2003**, *86*, 782.
(52) Zhu, P. X.; Masuda, Y.; Koumoto, K. *Biomaterials* **2004**, *25*, 3915.
(53) Tarasevich, B. J.; Chusuei, C. C.; Allara, D. L. *J. Phys. Chem. B* **2003**, *107*, 10367.
(54) Wilson, R. M.; Elliott, J. C.; Dowker, S. E. P. *Am. Miner.* **1999**, *84*, 1406.

phosphorus density instead of crystallite coalescence. The further increase in the M_2 value from the 3-hr sample (6.4 $\pm$ 0.3) to the 21.5-hr sample (7.4 $\pm$ 0.4) can be ascribed to the formation of the crystalline phase, where the phosphate units are packed closer than those in amorphous state. In principle, the ^{31}P-^{31}P second moment of the minerals deposited on the glass surface can also be obtained by measuring the attenuation of spin−echo intensities as a function of inter-pulse delay under static condition.[48] Although our method is more involved in the experimental setup, it offers a lot better spectral resolution than the spin−echo approach, which has to be carried out under static conditions.

Formation of Apatite. Initially, the phosphorus density of the mineral layer deposited on the glass surface was substantially smaller than that in crystalline HAp. After 1 h of SBF soaking, there was a significant increase in the phosphorus density of the phosphorus species. Presumably an amorphous layer with constituents similar to HAp had formed on the glass surface (Figure 10). The water molecules in the amorphous layer had restricted motion only and some of them were hydrogen-bonded to the neighboring PO_4^{3-} ions, possibly in equilibrium with HPO_4^{2-} (Figure 8). The amorphous layer grew continuously as the soaking time increased. The only noticeable change in the period between 1-hr and 3-hr is that the amount of structural water relative to the phosphate content decreased considerably. This interpretation is consistent with the corresponding increase in the $T_{1\rho}^H$ values (Figure 9). After 6 h of SBF soaking, a considerable amount of apatite nanocrystals had been formed (Figures 6). The deposition rate of PO_4^{3-} ions on the glass surface hence increased considerably between 6 and 12 h, presumably due to the epitaxial crystal growth. The PO_4^{3-} deposition was basically completed after 12 h of SBF soaking as evidenced by the moderate increase in phosphate mass percentage after 21.5 h. Overall, our data favor the Hench mechanism concerning the precipitation and crystallization of the phosphate ions and are consistent with the recent results of X-ray spectroscopic study.[9] In view of the fact that calcite is present at the early stage of apatite formation (Figure 4), one should be cautious in interpreting the C−O stretching mode observed in the FT-IR spectra because calcite also has an IR absorption at 875 cm^{-1}. Nevertheless, another characteristic absorption of calcite (a weaker absorption at 714 cm^{-1}) is not found in our FT-IR spectra.[55]

As an alternative to the Hench mechanism, it has been argued that the gel-silica may provide epitaxial sites for the growth of HAp.[56] However, if it were the case for our glass system, the line widths of the ^{31}P signals would not have such a big variation as illustrated in Figure 6. On the other hand, Hayakawa et al. reported that the ^{31}P signals indeed have very similar line widths for Na_2O (20%)-SiO_2 (80%) glasses with different soaking periods in SBF. In addition, recent X-ray photoelectron spectroscopy and TEM-EDX studies on a similar glass system shows that the formation of calcium silicate precede the precipitation of calcium phosphate on the glass surface.[39,57] Therefore, it is not clear if a universal mechanism exists for the apatite formation on all kinds of bioactive glasses. Also, since the nature of the calcium phosphate phases precipitated from the SBF solution depends strongly on the solution composition, it is helpful to maintain a more constant SBF composition for studies relevant to in-vivo applications.[58]

Acknowledgment. This work was supported by a grant from the National Science Council under the contract number NSC 93-2113-M-002-016. The insightful and detailed comments of the anonymous reviewers are gratefully acknowledged.

Supporting Information Available: Detailed assignment of the XRD pattern of the 1-hr and 3-hr samples, LG-CP HETCOR spectra of the 3-hr and 6-hr samples, fittings of the CPMAS raw data, fittings of the DQ raw data. This material is available free charge via the Internet at http://pubs.acs.org.

CM050654C

(55) Aizenberg, J.; Muller, D. A.; Grazul, J. L.; Hamann, D. R. *Science* **2003**, *299*, 1205.
(56) Karlsson, K. H.; Froberg, K.; Riingbom, T. *J. Non-Cryst. Solids* **1989**, *112*, 69.
(57) Takadama, H.; Kim, H. M.; Kokubo, T.; Nakamura, T. *J. Am. Ceram. Soc.* **2002**, *85*, 1933.
(58) Vallet-Regi, M.; Ragel, C. V.; Salinas, A. J. *Eur. J. Inorg. Chem.* **2003**, 1029.
(59) Mathew, M.; Brown, W. E.; Schroeder, L. W.; Dickens, B. *J. Cryst. Spec. Res.* **1988**, *18*, 235.